J Mater Sci (2017) 52:13356–13364

Biomaterials

RGD-conjugated titanium dioxide nanoparticles: targeted near-infrared photothermal therapy for $\alpha_v\beta_3$ integrin overexpressed cancer cells

Heng Zhao[1], Min Wang[1], Ping Zhou[1], Quan Wang[1], Zhiguo Zhou[1,*], Danli Wang[1], Hong Yang[1], and Shiping Yang[1,*]

[1] *The Key Laboratory of Resource Chemistry of Ministry of Education, Shanghai Key Laboratory of Rare Earth Functional Materials, and Shanghai Municipal Education Committee Key Laboratory of Molecular Imaging Probes and Sensors, Shanghai Normal University, Shanghai 200234, China*

Received: 27 March 2017
Accepted: 11 April 2017
Published online: 30 August 2017

ABSTRACT

Photothermal agents, which can convert near-infrared light into heat with a minimal attenuation of the energy and prevent undesirable thermal damage to healthy tissue, provided an opportunity for accurate heat delivery to desired sites. Herein, we designed cyclo(Arg-Gly-Asp-D-Tyr-Lys) peptide c(RGDyK)-conjugated TiO_2 nanoparticles (TiO_2-RGD NPs) with an ideal biocompatibility and targeting property. TiO_2-RGD NPs exhibited intense absorbance in near-infrared region, a high stability in physiological conditions, and the photothermal conversion efficiency of ~38.5%. Due to the specific affinity between c(RGDyK) and $\alpha_v\beta_3$ integrin, TiO_2-RGD NPs showed the high targeting property for U87-MG cells with overexpression of $\alpha_v\beta_3$ integrin. After incubation with TiO_2-RGD NPs (100 μg/mL) and under 808 nm near-infrared laser irradiation (1 W/cm^2), the viability of MCF-7 cells by deficient expression of $\alpha_v\beta_3$ integrin was ~71%, while the viability of U87-MG decreased to ~31%, which have been demonstrated as an effective targeting photothermal therapy agent.

Introduction

Photothermal therapy (PTT) based on photothermal agents (PTAs) with the near-infrared (NIR) absorption has aroused an increasing attention in the past years due to their advantages of eliminating tumors noninvasively [1] and enhances the therapeutic efficacy to cancer selectively [2]. Nanoparticulated PTAs are including gold nanomaterials [3–9] such as gold nanorods, gold nanoshells, gold nanocages, and gold nanocrystals and carbon nanomaterials [10–12] such as graphene nanomesh, nanographene oxide, graphene quantum dots, and carbon nanotubes, copper-based nanoparticles [13–15], and other inorganic nanoparticles [16–18]. To perform the clinical application of PTT in the future, it is necessary to develop highly efficient and biocompatible PTAs.

Address correspondence to E-mail: zgzhou@shnu.edu.cn; shipingy@shnu.edu.cn

DOI 10.1007/s10853-017-1083-9

On January 20, 2015, Obama announced a precision medicine initiative in his state of the union address [19]. Thereafter, precision therapy has been an emerging approach for personal medicine. As for precise photothermal therapy, it is one of the most important issues to develop PTAs with targeting property in order to secure the irreversible destruction of tumor cells without damage to adjacent healthy cells. To perform the targeting property of PTAs to tumor, receptor-mediated recognition has been regarded as an effective strategy. According to Kessler's work [20], cyclo(Arg-Gly-Asp-D-Tyr-Lys) peptide c(RGDyK) is a particularly effective ligand to bind $\alpha_v\beta_3$ integrin receptors which are highly expressed on blood vessels in tumor [21]. Therefore, it is effective to conjugate c(RGDyK) onto nanoparticles to target $\alpha_v\beta_3$ integrin overexpressed tumor. [22–24] Our group has developed RGD-conjugated magnetic nanoparticles for targeted photothermal therapy and imaging in vivo. [16, 25–27].

TiO_2, a famous wide-band semiconductor, has been explored extensively in the field of energy conversion and photocatalysis due to the outstanding of electron transport, charge separation, and UV light absorption [28–30]. With the advantage of low toxicity, it has been also applied in the field of sonodynamic therapy [31–35] and UV-induced photodynamic therapy [36]. As far as we know, few studies have been reported about the near-infrared (NIR)-driven targeting phototherapy.

To overcome the less penetration depth of UV light, we prepared TiO_2 nanoparticles (TiO_2 NPs) with the high temperature thermal decomposition method. Importantly, due to the absorption of electrons localized on Ti(III) sites and free electrons in the conduction band, the synthesized TiO_2 NPs exhibited an intense absorbance in the NIR region. Considering targeting property of c(RGDyK) to $\alpha_v\beta_3$ integrin, c(RGDyK) was covalently conjugated to TiO_2 NPs with a PEG liker by a strain-promoted click chemistry. By use of NIR-driven photothermal therapy, targeted photothermal therapy was performed for $\alpha_v\beta_3$ integrin overexpressed cancer cells (Scheme 1).

Materials and methods

Materials

Titanium (IV) fluoride (TiF_4, 99%), nitrosonium tetrafluoroborate ($NOBF_4$), 1-octadecene (90%) (1-ODE), 1-octadecanol (1-ODOL, 97%), *N,N*-dimethylformamide (DMF), toluene, hexane, acetone, ethanol, and 2-propanol were purchased from Acros Organics. Oleylamine (OLAM, 70%), oleic acid (OLAC, 90%), and acetonitrile were purchased from Sigma Aldrich. Dibenzylcyclooctyne-PEG_{2000} (DBCO-PEG_{2000}) and dibenzylcyclooctyne-PEG_{2000}-NHS (DBCO-PEG_{2000}-NHS) were purchased from Nanocs Inc. Cyclo(Arg-Gly-Asp-D-Tyr-Lys) peptide c(RGDyK) was purchased from Peptide International, Inc. All reagents were used without further purification. Water used in all experiments was purified using a Milli-Q Plus 185 water purification system (Millipore, Bedford, MA) with resistivity higher than 18 MΩ·cm. Cellulose dialysis membranes (molecular weight cut-off, MWCO = 14 000) were acquired from Fisher.

Preparation of azide functionalized TiO_2 nanoparticles (TiO_2–N_3 NPs)

TiO_2 nanoparticles could be synthesized according to the literature [37]. 0.1 g of $NOBF_4$ was dissolved in 10 mL DMF to form a yellow solution. The yellow solution was mixed with a hexane dispersion of TiO_2 NPs (10 mL). Then, 2 mL, the mixture solution of toluene and hexane (1:1, v/v), was added and centrifuged. After centrifugation, blue TiO_2-BF_4 NPs were obtained. Secondly, 20 mg 2-azido-1-(3,4-dihydroxyphenyl)ethanone was dissolved in 10 mL DMF, and adjusted pH value of the solution to 10 using tetrabutyl ammonium hydroxide, which was mixed with the above blue precipitation. After reaction for 8 h, the mixture was centrifuged to obtain TiO_2–N_3 NPs.

Synthesis of PEGylated functionalized TiO_2 nanoparticles (TiO_2-PEG NPs)

Two milligrams of DBCO-PEG_{2000} was added in the ethanol solution of TiO_2–N_3 NPs (5 mL, 1 mg/mL), then after the reaction at room temperature for 24 h, the solution was centrifuged to obtain TiO_2-PEG NPs.

Preparation of RGD-conjugated TiO_2 nanoparticles (TiO_2-RGD NPs)

Two milligrams of DBCO-PEG_{2000} was added into the mixture solution with the ethanol solution of TiO_2-N_3 NPs (5 mL, 1 mg/mL) and the DMF solution of

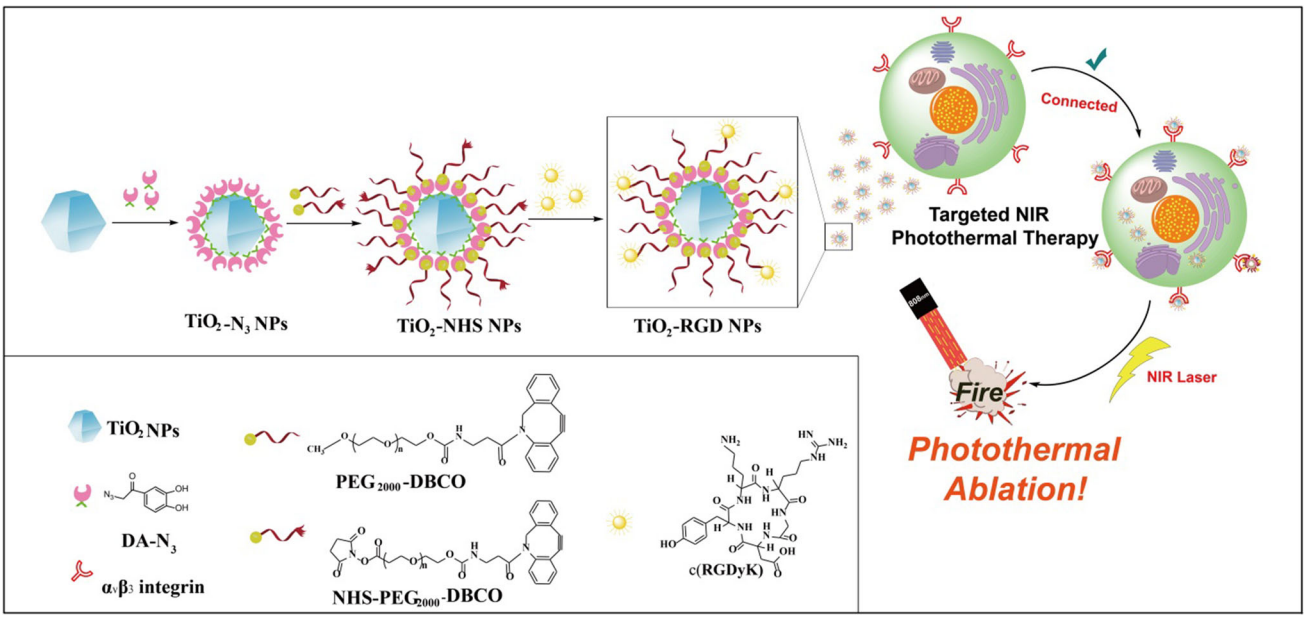

Scheme 1 Schematic illustration for the design of TiO_2-RGD NPs and targeted near-infrared photothermal therapy for $\alpha_v\beta_3$ integrin overexpressed cancer cells.

DBCO-PEG_{2000}-NHS (0.25 mL, 2 mg/mL). After the reaction at room temperature for 24 h, the mixed solution was centrifuged to obtain TiO_2-NHS NPs. The PBS solution of c(RGDyK) (2 mL, 1 mg/mL) was added in the aqueous solution of TiO_2-NHS NPs (0.5 mL, 1 mg/mL) for the reaction for 4 h. Then, the mixed solution was dialyzed in ultra-pure water for 48 h. After that the solution was transferred to a vial and saved at 4 °C.

Photothermal experiments in solution

The aqueous suspension of TiO_2-PEG NPs with different concentrations was put in a cuvette with an optical path length of 1.0 cm. Then the cuvette was illuminated by an 808-nm laser with a power density of 0.6 W/cm^2 for 10 min. The change of temperature was monitored by a digital thermocouple device.

In vitro toxicity

U87-MG (human glioblastoma cells), MCF-7 (human breast cancer cells), and L929 cells (mouse fibroblast cells) were cultured in DMEM or RPMI 1640 medium (Thermo, USA) supplemented with 10% FBS (Gibco, USA) and 1% penicillin–streptomycin (Thermo, USA) at 37 °C under a 5% CO_2 atmosphere. Cells were generally plated in cell culture flasks and allowed to adhere for 24 h, then harvested by treatment with 0.25% trypsin–EDTA solution (Gibco, USA). U87-MG, MCF-7 and L929 cells were plated in 96-well microplates with a density of 10^4 cells/well. After the incubation for 12 h, cells were incubated with TiO_2-RGD NPs with different concentrations (10, 20, 50, 100, and 200 μg/mL), respectively. The cytotoxicity was assessed with a standard 3-[4, 5-Dimethylthiazol-2-yl]-2, 5-diphenyltetrazolium bromide (MTT) method.

In vitro photothermal therapy (PTT)

U87-MG and MCF-7 cells were incubated with TiO_2-PEG NPs or TiO_2-RGD NPs (100 μg/mL) for different incubation time (0, 2, 4, 8, 12, and 24 h, respectively), followed by washing with phosphate buffer solution (PBS, pH 7.4) for three times. After an 808-nm laser irradiation (1.0 W/cm^2) for 10 min, MTT assay was further used after incubation for another 1 h.

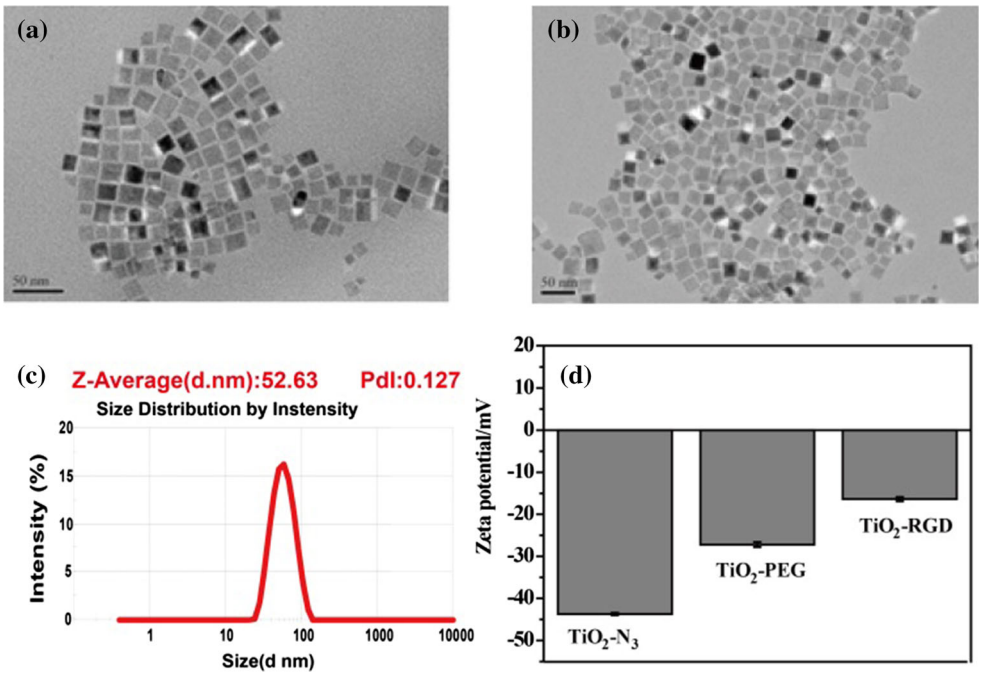

Figure 1 TEM images of TiO_2 NPs (**a**) and TiO_2-RGD NPs (**b**), respectively. **c** The hydrodynamic diameter of TiO_2-RGD NPs dispersed in water. **d** The zeta potential of TiO_2–N_3, TiO_2-PEG, and TiO_2-RGD NPs, respectively.

Characterization

TEM images were collected on a JEOL JEM-2010 transmission electron microscope operating at an accelerating voltage of 200 kV. FT-IR spectra were collected using a Nicolet Avatar 370 FT-IR spectrometer in the 400–4000 cm^{-1} region. The samples were pelletized with KBr before measurements. The surface potential and hydration radius were measured using a Malvern Zetasizer Nano ZS model ZEN3690 (Worcestershire, U.K.) equipped with a standard 633 nm laser. The concentration of Ti was determined by inductively coupled plasma mass spectrometry (ICP-MS, VISTAMPXICP VARIAN).

Results and discussion

Synthesis and characterization of functionalized TiO_2 NPs

According to the literature, TiO_2 NPs was synthesized with a high uniform tetragonal bipyramidal morphology of the lateral size of ~17 nm (Fig. 1a). [38] The pure anatase phase was confirmed by powder X-ray diffraction (PXRD) (Fig.S1). The binding energy of $Ti_{2p3/2}$ peak located at 458.9 eV suggested the existence of Ti(III) (Fig.S2). To perform water solubility and targeting property of TiO_2 NPs, TiO_2 NPs were modified by 2-azido-1-(3,4-dihydroxyphenyl)ethanone (DA–N_3) through a typical process of ligand-exchange reaction, in which nitrosonium tetrafluoroborate ($NOBF_4$) was used to replace the ligand on the surface of TiO_2 NPs. [39] The azide stretching frequency located at 2100 cm^{-1} in the FT-IR spectrum (Fig.S3) confirmed the existence of azide on the surface of TiO_2 NPs. From the thermogravimetric analysis (TGA), the content of DA-N_3 on the surface of TiO_2 NPs was ~15% (Fig.S4). Followed by strain-promoted click chemistry, DBCO-PEG_{2000} and DBCO-PEG_{2000}-NHS were grafted on TiO_2 NPs (Fig.S5) [40]. Lastly, RGD was conjugated on the surface of TiO_2 NPs with the amide bond to obtain targeted TiO_2-RGD NPs (Fig.S5). As shown from TEM (Fig. 1b), TiO_2-RGD NPs had a mean edge length of ~19 nm, which was similar to that of TiO_2 NPs. The hydrodynamic diameter of TiO_2-RGD NPs dispersed in water was about 53 nm (Fig. 1c), which was similar to that of TiO_2-PEG NPs (Fig.S6). The surface potential increased to −15.1 mV for TiO_2-RGD NPs comparing with −30 mV of TiO_2-PEG NPs due to the positive charge of RGD (Fig. 1d), which could be explained by the surface coverage of TiO_2 NPs with RGD. To verify its stability under physiological conditions, diameter changes of TiO_2-RGD NPs were monitored in water, PBS, 1640 plus 10% fetal bovine serum (FBS) as simulated in vivo plasma (Fig. S7). The diameters of TiO_2-RGD NPs

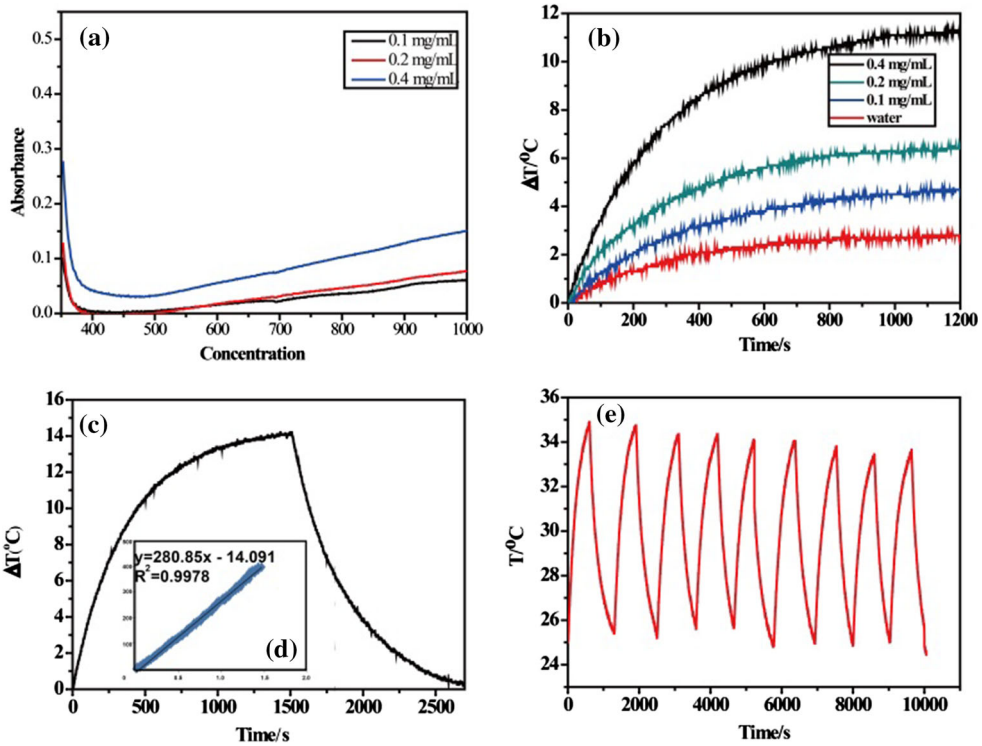

Figure 2 **a** Photothermal effect of different concentrations of TiO_2-PEG NPs (100, 200, and 400 μg/mL, respectively). **b** Temperature changes of with different concentrations TiO_2-PEG NPs (0, 100, 200, and 400 μg/mL, respectively) under an 808-nm laser irradiation (0.60 W/cm^2). **c** Photothermal efficiency of TiO_2-PEG NPs (400 μg/mL) under an 808-nm laser irradiation (0.60 W/cm^2). **d** Plot of cooling time versus negative natural logarithm of the temperature driving force obtained from the cooling stage as shown in (**c**). **e** Photothermal cycle curve of TiO_2-PEG NPs.

were almost no changes in physiological conditions within one week. Moreover, TiO_2-PEG NPs also exhibited good stability at different pH values (pH = 5.4, 7.0, 8.4, and 10.0, respectively) (Fig. S8). The fact suggested that TiO_2-RGD NPs should be stable enough for further in vivo application.

Due to the absorption of electrons localized on Ti(III) sites and free electrons in the conduction band, TiO_2 NPs exhibited an appreciable absorbance in the NIR region (Fig. 2a). [38] A broad absorption in the NIR region of TiO_2 NPs encouraged us to investigate their photothermal property. The photothermal effect of different concentrations of TiO_2-PEG NPs (100, 200 and 400 μg/mL, respectively) was evaluated by an 808-nm NIR laser irradiation (0.60 W/cm^2) for 600 s (Fig. 2b). The solution of TiO_2-PEG NPs showed a rapid increase in temperature during the laser irradiation. In contrast, under the same experimental condition, the temperature of water displayed no apparent increase. At the concentration of 400 mg/mL, the temperature was raised by 11.8 °C after an 808-nm laser irradiation. The decrease in the concentration of TiO_2-PEG NPs will slow down the temperature increment, illustrating that the thermal energy was converted by the NIR optical absorbance of TiO_2-PEG NPs. According to the calculation method reported by the literature, the photothermal conversion efficiency of TiO_2-PEG NPs was ~38.5% (Fig. 2c) [41]. Meanwhile, the photothermal stability of TiO_2-PEG NPs was investigated by cycles of 808-nm laser on/off of aqueous solution of TiO_2-PEG NPs. After nine repeated cycles of laser on/off, the temperature increase in TiO_2-PEG NPs exhibited no obvious changes (Fig. 2e). Furthermore, the photothermal stability of TiO_2-PEG

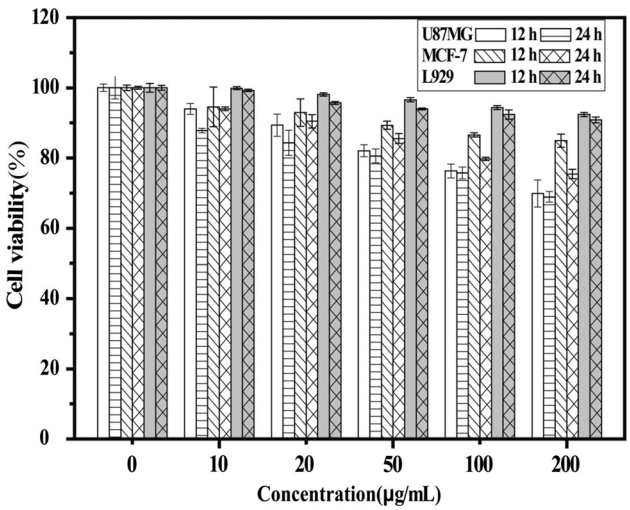

Figure 3 Cell viabilities of U87-MG, MCF-7, and L929 cells after being incubated with TiO_2-RGD NPs for 12 and 24 h, respectively.

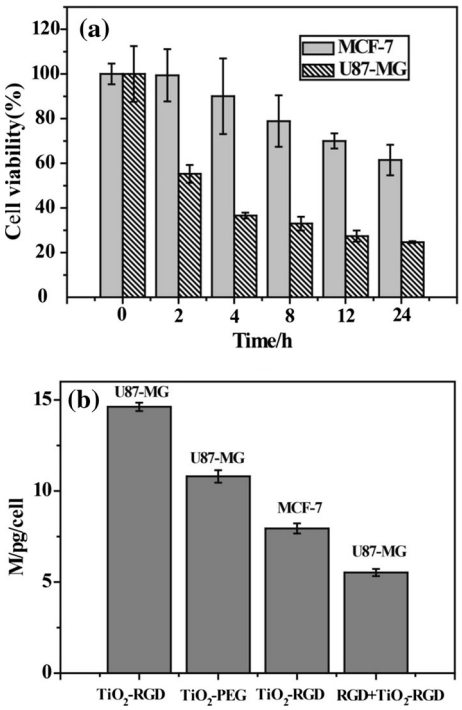

Figure 4 **a** Cell viabilities of U87-MG and MCF-7 cells incubation with TiO_2-RGD NPs (100 μg/mL) for different time (0, 2, 4, 8, 12, and 24 h, respectively), then irradiated with an 808-nm laser. **b** The cellular uptake of Ti per cell of U87-MG and MCF-7 cells quantitatively measured by ICP-MS analysis.

NPs can also be confirmed by absorption spectra having nearly no obvious changes before and after laser irradiation (Fig.S9). These data all clearly demonstrated that TiO_2-PEG NPs have high photothermal conversion efficiency and photothermal stability during NIR irradiation.

In vitro cytotoxicity of TiO_2-RGD NPs

MTT assay was performed to quantitatively examine the viabilities of U87-MG cells ($\alpha_v\beta_3$ integrin overexpression). As a control, we also examined the viability of MCF-7 cells (which express low level of $\alpha_v\beta_3$ integrin) and normal cells (L929 cells). As shown in Fig. 3, no significant cytotoxicity of TiO_2-RGD NPs was observed for normal cells even at a high concentration of 200 μg/mL. However, TiO_2-RGD NPs showed relatively higher cytotoxicity to tumor cells than that of normal cells (L929 cells) especially at a high concentration of 200 μg/mL, which was due to the high specific targeting ability of TiO_2-RGD NPs and the high cytotoxicity as a result.

Targeted property of TiO_2-RGD NPs

To confirm the targeting ability of TiO_2-RGD NPs in vitro, cell viabilities of U87-MG and MCF-7 cells were measured after the incubation with TiO_2-RGD NPs (100 μg/mL) for different time (0, 2, 4, 8, 12, and 24 h, respectively) and then an 808-nm laser irradiation (1.0 W/cm^2) for 10 min, respectively (Fig. 4a). After the incubation for 2 h and exposed to an 808-nm laser irradiation, the viability of U87-MG cells decreased to ~55%. However, under the same conditions, the viability of MCF-7 cells showed a negligible change. With the incubated time increased from 4 to 24 h, the viability of U87-MG cells decreased from 35 to 25%. These results demonstrated that TiO_2-RGD NPs owned the perfect targeted photothermal effect.

To further evaluate the targeting property, the cellular uptake of TiO_2-RGD NPs in U87-MG cells, block, and control experiments was quantitatively determined by the amount of Ti per cells measured by ICP-MS analysis (Fig. 4b). For the block experiment (RGD + TiO_2-RGD), free RGD (50 μg/mL) was pre-incubated with U87-MG cells and then cultured with TiO_2-RGD NPs (100 μg/mL), and the uptake of Ti in U87-MG cells was decreased to 5.52 ± 0.20 pg/cell from 14.6 ± 0.23 pg/cell in cells being incubated with only TiO_2-RGD NPs. With the incubation of TiO_2-RGD NPs (100 μg/mL) for MCF-7 cells, relatively low cellular uptake of 7.94 ± 0.28 pg/cell Ti was measured. When U87-MG cells were incubated with TiO_2-PEG NPs (100 μg/mL) with no-targeting property, the uptake of Ti was 10.8 ± 0.34 pg/cell, which was less than that of TiO_2-RGD NPs. These results indicated that the cellular uptake of TiO_2-RGD NPs is mainly mediated by RGD endocytosis.

In vitro targeted photothermal therapy

The targeting photothermal therapy was further studied in vitro. U87-MG and MCF-7 cells were incubated with the concentration of TiO_2-RGD for 4 h, respectively, and then irradiated by an 808-nm laser (1.0 W/cm^2) for 10 min (Fig. 5). The viability of U87-MG cells decreased to ~31% (TiO_2-RGD + L). As for experiment group, TiO_2-RGD NPs were enriched greatly in U87-MG cells due to the targeting property of c(RGDyK). Therefore, a perfect photothermal therapy was realized. However, the viability of MCF-7 cells was ~71% (TiO_2-RGD + L). For MCF-7 cells with $\alpha_v\beta_3$ integrin deficient expression,

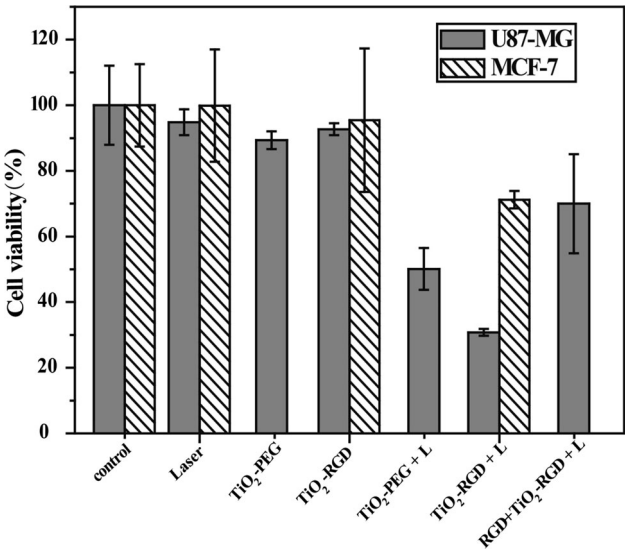

Figure 5 Cell viabilities of U87-MG and MCF-7 cells under different treating conditions. The incubating concentration of TiO_2-RGD NPs or TiO_2-PEG NPs is 100 μg/mL (laser is abbreviated as "L").

TiO_2-RGD NPs behaved no-targeting property, leading to poor photothermal therapy effect. Furthermore, the viability of U87-MG cells incubated with TiO_2-PEG NPs (100 μg/mL) for 4 h and under the same irradiation was ~50% (TiO_2-PEG + L). Similarly, TiO_2-PEG NPs with no c(RGDyK) also showed no-targeting property and resulted in obvious the photothermal therapy effect under the laser irradiation. There was no obvious decrease in the viability for U87-MG cells and/or MCF-7 cells only incubated with TiO_2-RGD NPs and TiO_2-PEG NPs or only irradiated by an 808-nm laser, respectively. As control groups, laser only, TiO_2-PEG only, and TiO_2-RGD NPs only groups showed low cytotoxicity to U87-MG cells and MCF-7 cells. Furthermore, after an 808-nm irradiation, the viability of the block group (RGD + TiO_2-RGD + L) was also higher than that of the experimental group. The block group was also conformed the targeting property of TiO_2-RGD NPs therapy. The data furthermore demonstrated that the perfect targeting effect of TiO_2-RGD NPs should be an ideal platform for cancer cells.

Conclusions

In summary, we have successfully synthesized c(RGDyK) conjugated PEGylated TiO_2 NPs for targeting photothermal therapy of cancer cells by use of the specific affinity between c(RGDyK) and $\alpha_v\beta_3$ integrin combined a seeded growth method and strain-promoted click chemistry. Our procedure offers a simple route to develop novel functional TiO_2 NPs and opens up new ideas for multiple applications of TiO_2 NPs in the field of biomedical application.

Acknowledgements

This work was partially supported by National Natural Science Foundation of China (Nos. 21371122, and 21571130, 21671135), the Ministry of Education of China (PCSIRT_IRT_16R49), and International Joint Laboratory on Resource Chemistry of Ministry of Education (IJLRC).

Electronic supplementary material: The online version of this article (doi:10.1007/s10853-017-1083-9) contains supplementary material, which is available to authorized users.

References

[1] Lin M, Wang D, Liu S, Huang T, Sun B, Cui Y, Zhang D, Sun H, Zhang H, Sun H, Yang B (2015) Cupreous complex-loaded chitosan nanoparticles for photothermal therapy and chemotherapy of oral epithelial carcinoma. ACS Appl Mater Interfaces 7(37):20801–20812. doi:10.1021/acsami.5b05866

[2] Wang S, Tian Y, Tian W, Sun J, Zhao S, Liu Y, Wang C, Tang Y, Ma X, Teng Z, Lu G (2016) Selectively sensitizing malignant cells to photothermal therapy using a CD44-targeting heat shock protein 72 depletion nanosystem. ACS Nano 10(9):8578–8590. doi:10.1021/acsnano.6b03874

[3] Kang S, Bhang SH, Hwang S, Yoon JK, Song J, Jang HK, Kim S, Kim BS (2015) Mesenchymal stem cells aggregate and deliver gold nanoparticles to tumors for photothermal therapy. ACS Nano 9(10):9678–9690. doi:10.1021/acsnano.5b02207

[4] Ke H, Wang J, Dai Z, Jin Y, Qu E, Xing Z, Guo C, Yue X, Liu J (2011) Gold-nanoshelled microcapsules: a theranostic agent for ultrasound contrast imaging and photothermal therapy. Angew Chem 50(13):3017–3021. doi:10.1002/anie.201008286

[5] Liu H, Chen D, Li L, Liu T, Tan L, Wu X, Tang F (2011) Multifunctional gold nanoshells on silica nanorattles: a platform for the combination of photothermal therapy and chemotherapy with low systemic toxicity. Angew Chem 50(4):891–895. doi:10.1002/anie.201002820

[6] Rengan AK, Bukhari AB, Pradhan A, Malhotra R, Banerjee R, Srivastava R, De A (2015) In vivo analysis of biodegradable liposome gold nanoparticles as efficient agents for photothermal therapy of cancer. Nano Lett 15(2):842–848. doi:10.1021/nl5045378

[7] Tsai MF, Chang SH, Cheng FY, Shanmugam V, Cheng YS, Su CH, Yeh CS (2013) Au nanorod design as light-absorber in the first and second biological near-infrared windows for in vivo photothermal therapy. ACS Nano 7(6):5330–5342. doi:10.1021/nn401187c

[8] Zhang L, Chen Y, Li Z, Li L, Saint-Cricq P, Li C, Lin J, Wang C, Su Z, Zink JI (2016) Tailored synthesis of octopus-type janus nanoparticles for synergistic actively-targeted and chemo-photothermal therapy. Angew Chem 55(6):2118–2121. doi:10.1002/anie.201510409

[9] Zheng T, Li GG, Zhou F, Wu R, Zhu JJ, Wang H (2016) Gold-nanosponge-based multistimuli-responsive drug vehicles for targeted chemo-photothermal therapy. Adv Mater 28(37):8218–8226. doi:10.1002/adma.201602486

[10] Yao X, Niu X, Ma K, Huang P, Grothe J, Kaskel S, Zhu Y (2016) Graphene quantum dots-capped magnetic mesoporous silica nanoparticles as a multifunctional platform for controlled drug delivery, magnetic hyperthermia, and photothermal therapy. Small. doi:10.1002/smll.201602225

[11] Akhavan O, Ghaderi E (2013) Graphene nanomesh promises extremely efficient in vivo photothermal therapy. Small 9(21):3593–3601. doi:10.1002/smll.201203106

[12] Hs DJ, Kong WH, Sung DK, Lee MY, Beack SE, Keum DH, Kim KS, Yun SH, Hahn SK (2014) Nanographene oxide-hyaluronic acid conjugate for photothermal ablation therapy of skin cancer. ACS Nano 8(1):260–268. doi:10.1021/nn405383a

[13] Mou J, Li P, Liu C, Xu H, Song L, Wang J, Zhang K, Chen Y, Shi J, Chen H (2015) Ultrasmall Cu_{2-x} S nanodots for highly efficient photoacoustic imaging-guided photothermal therapy. Small 11(19):2275–2283. doi:10.1002/smll.201403249

[14] Liu J, Wang P, Zhang X, Wang L, Wang D, Gu Z, Tang J, Guo M, Cao M, Zhou H, Liu Y, Chen C (2016) Rapid degradation and high renal clearance of Cu3BiS3 nanodots for efficient cancer diagnosis and photothermal therapy in Vivo. ACS Nano 10(4):4587–4598. doi:10.1021/acsnano.6b00745

[15] Zhang S, Sun C, Zeng J, Sun Q, Wang G, Wang Y, Wu Y, Dou S, Gao M, Li Z (2016) Ambient aqueous synthesis of ultrasmall PEGylated Cu_{2-x} Se nanoparticles as a multifunctional theranostic agent for multimodal imaging guided photothermal therapy of cancer. Adv Mater 28(40):8927–8936. doi:10.1002/adma.201602193

[16] Wang J, Zhao H, Zhou Z, Zhou P, Yan Y, Wang M, Yang H, Zhang Y, Yang S (2016) MR/SPECT imaging guided photothermal therapy of tumor-targeting Fe@Fe_3O_4 nanoparticles in vivo with low mononuclear phagocyte uptake. ACS Appl Mater Interfaces 8(31):19872–19882. doi:10.1021/acsami.6b04639

[17] Wang J, Zhou Z, Wang L, Wei J, Yang H, Yang S, Zhao J (2015) $CoFe_2O_4$@$MnFe_2O_4$/polypyrrole nanocomposites for in vitro photothermal/magnetothermal combined therapy. RSC Adv 5(10):7349–7355. doi:10.1039/c4ra12733a

[18] Guo Z, Zou Y, He H, Rao J, Ji S, Cui X, Ke H, Deng Y, Yang H, Chen C, Zhao Y, Chen H (2016) Bifunctional platinated nanoparticles for photoinduced tumor ablation. Adv Mater. doi:10.1002/adma.201602738

[19] Church GM (2015) Precision chemistry for precision medicine. ACS Cent Sci 1(1):11–13. doi:10.1021/acscentsci.5b00088

[20] Haubner R, Gratias R, Diefenbach B, Goodman SL, Jonczyk A, Kessler H (1996) Structural and functional aspects of RGD-containing cyclic pentapeptides as highly potent and selective integrin $\alpha_V\beta_3$ antagonists. J Am Chem Soc 118(32):7461–7472. doi:10.1021/ja9603721

[21] Desgrosellier JS, Cheresh DA (2010) Integrins in cancer: biological implications and therapeutic opportunities. Nat Rev Cancer 10(1):9

[22] Cai W, Shin D-W, Chen K, Gheysens O, Cao Q, Wang SX, Gambhir SS, Chen X (2006) Peptide-labeled near-infrared quantum dots for imaging tumor vasculature in living subjects. Nano Lett 6(4):669–676. doi:10.1021/nl052405t

[23] Danhier F, Breton AL, Préat V (2012) RGD-based strategies to target alpha(v) beta(3) Integrin in cancer therapy and diagnosis. Mol Pharm 9(11):2961

[24] Xie J, Chen K, Lee H-Y, Xu C, Hsu AR, Peng S, Chen X, Sun S (2008) Ultrasmall c(RGDyK)-coated Fe_3O_4 nanoparticles and their specific targeting to integrin $\alpha_v\beta_3$-rich tumor cells. J Am Chem Soc 130(24):7542–7543. doi:10.1021/ja802003h

[25] Yang H, Qin C, Yu C, Lu Y, Zhang H, Xue F, Wu D, Zhou Z, Yang S (2014) RGD-conjugated nanoscale coordination polymers for targeted T1- and T2-weighted magnetic resonance imaging of tumors in Vivo. Adv Func Mater 24(12):1738–1747. doi:10.1002/adfm.201302433

[26] An L, Hu H, Du J, Wei J, Wang L, Yang H, Wu D, Shi H, Li F, Yang S (2014) Paramagnetic hollow silica nanospheres for in vivo targeted ultrasound and magnetic resonance imaging. Biomaterials 35(20):5381–5392. doi:10.1016/j.biomaterials.2014.03.030

[27] Yang H, Zhuang Y, Sun Y, Dai A, Shi X, Wu D, Li F, Hu H, Yang S (2011) Targeted dual-contrast T_1- and T_2-weighted magnetic resonance imaging of tumors using multifunctional gadolinium-labeled superparamagnetic iron oxide nanoparticles. Biomaterials 32(20):4584–4593. doi:10.1016/j.biomaterials.2011.03.018

[28] Choi J, Song S, Horantner MT, Snaith HJ, Park T (2016) Well-defined nanostructured, single-crystalline TiO_2 electron transport layer for efficient planar perovskite solar cells. ACS Nano 10(6):6029–6036. doi:10.1021/acsnano.6b01575

[29] Zhang J, Jin X, Morales-Guzman PI, Yu X, Liu H, Zhang H, Razzari L, Claverie JP (2016) Engineering the absorption and field enhancement properties of Au-TiO_2 nanohybrids via whispering gallery mode resonances for photocatalytic water splitting. ACS Nano 10(4):4496–4503. doi:10.1021/acsnano.6b00263

[30] Lu X, Chen A, Luo Y, Lu P, Dai Y, Enriquez E, Dowden P, Xu H, Kotula PG, Azad AK, Yarotski DA, Prasankumar RP, Taylor AJ, Thompson JD, Jia Q (2016) Conducting interface in oxide homojunction: understanding of superior properties in black TiO_2. Nano Lett 16(9):5751–5755. doi:10.1021/acs.nanolett.6b02454

[31] Deepagan VG, You DG, Um W, Ko H, Kwon S, Choi KY, Yi GR, Lee JY, Lee DS, Kim K, Kwon IC, Park JH (2016) Long-circulating Au-TiO_2 nanocomposite as a sonosensitizer for ROS-mediated eradication of cancer. Nano Lett. doi:10.1021/acs.nanolett.6b02547

[32] Harada A, Ono M, Yuba E, Kono K (2013) Titanium dioxide nanoparticle-entrapped polyion complex micelles generate singlet oxygen in the cells by ultrasound irradiation for sonodynamic therapy. Biomater Sci 1(1):65–73. doi:10.1039/c2bm00066k

[33] Ninomiya K, Ogino C, Oshima S, Sonoke S, Kuroda S, Shimizu N (2012) Targeted sonodynamic therapy using protein-modified TiO_2 nanoparticles. Ultrason Sonochem 19(3):607–614. doi:10.1016/j.ultsonch.2011.09.009

[34] Yamaguchi S, Kobayashi H, Narita T, Kanehira K, Sonezaki S, Kudo N, Kubota Y, Terasaka S, Houkin K (2011) Sonodynamic therapy using water-dispersed TiO_2-polyethylene glycol compound on glioma cells: comparison of cytotoxic mechanism with photodynamic therapy. Ultrason Sonochem 18(5):1197–1204. doi:10.1016/j.ultsonch.2010.12.017

[35] You DG, Deepagan VG, Um W, Jeon S, Son S, Chang H, Yoon HI, Cho YW, Swierczewska M, Lee S, Pomper MG, Kwon IC, Kim K, Park JH (2016) ROS-generating TiO_2 nanoparticles for non-invasive sonodynamic therapy of cancer. Scientific reports 6:23200. doi:10.1038/srep23200

[36] Miyoshi N, Kume K, Tsutumi K, Fukunaga Y, Ito S, Imamura Y, Bibin AB (2011) Application of titanium dioxide (TiO_2) nanoparticles in photodynamic therapy (PDT) of an experimental tumor. AIP Conf Proc 1415(1):21–23. doi:10.1063/1.3667210

[37] Goncalves RH, Schreiner WH, Leite ER (2010) Synthesis of TiO_2 nanocrystals with a high affinity for amine organic compounds. Langmuir ACS J Surf Coll 26(14):11657–11662. doi:10.1021/la1007473

[38] Gordon TR, Cargnello M, Paik T, Mangolini F, Weber RT, Fornasiero P, Murray CB (2012) Nonaqueous synthesis of TiO_2 nanocrystals using TiF_4 to engineer morphology, oxygen vacancy concentration, and photocatalytic activity. J Am Chem Soc 134(15):6751–6761. doi:10.1021/ja300823a

[39] Dong A, Ye X, Chen J, Kang Y, Gordon T, Kikkawa JM, Murray CB (2011) A generalized ligand-exchange strategy enabling sequential surface functionalization of colloidal nanocrystals. J Am Chem Soc 133(4):998–1006. doi:10.1021/ja108948z

[40] Guo Y, Yuan H, Rice WL, Kumar AT, Goergen CJ, Jokivarsi K, Josephson L (2012) The PEG-fluorochrome shielding approach for targeted probe design. J Am Chem Soc 134(47):19338–19341. doi:10.1021/ja309085b

[41] Liu Y, Ai K, Liu J, Deng M, He Y, Lu L (2013) Dopamine-melanin colloidal nanospheres: an efficient near-infrared photothermal therapeutic agent for in vivo cancer therapy. Adv Mater 25(9):1353–1359. doi:10.1002/adma.201204683